Flexible Graphene Field-Effect Transistors Encapsulated in Hexagonal Boron Nitride

Nicholas Petrone,[†] Tarun Chari,[‡] Inanc Meric,[‡] Lei Wang,[†] Kenneth L. Shepard,[‡] and James Hone*[,†]

[†]Department of Mechanical Engineering and [‡]Department of Electrical Engineering, Columbia University, New York, New York 10027, United States

ABSTRACT Flexible graphene field-effect transistors (GFETs) are fabricated with graphene channels fully encapsulated in hexagonal boron nitride (hBN) implementing a self-aligned fabrication scheme. Flexible GFETs fabricated with channel lengths of 2 μm demonstrate exceptional room-temperature carrier mobility (μ_{FE} = 10 000 cm^2 V^{-1} s^{-1}), strong current saturation characteristics (peak output resistance, r_0 = 2000 Ω), and high mechanical flexibility (strain limits of 1%). These values of μ_{FE} and r_0 are unprecedented in flexible GFETs. Flexible radio frequency FETs (RF-FETs) with channel lengths of 375 nm demonstrate μ_{FE} = 2200 cm^2 V^{-1} s^{-1} and r_0 = 132.5 Ω. Unity—current gain frequencies, f_T, and unity—power gain frequencies, f_{max}, reach 12.0 and 10.6 GHz, respectively. The corresponding ratio of cutoff frequencies approaches unity (f_{max}/f_T = 0.9), a record value for flexible GFETs. Intrinsic f_T and f_{max} are 29.7 and 15.7 GHz, respectively. The outstanding electronic characteristics are attributed to the improved dielectric environment provided by full hBN encapsulation of the graphene channel in conjunction with an optimized, self-aligned device structure. These results establish hBN as a mechanically robust dielectric that can yield enhanced electronic characteristics to a diverse array of graphene-based flexible electronics.

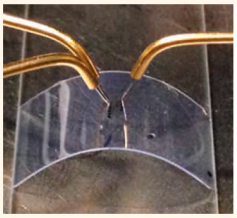

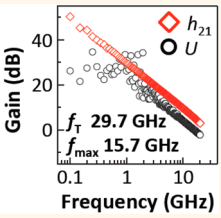

KEYWORDS: graphene · boron nitride · flexible electronics · radio frequency · FET

Flexible electronics that can adapt to curvilinear and malleable surfaces are required for applications such as conformal electronics, surface-mountable sensors, and bioelectronics.[1,2] Integration of wireless communication technology necessitates flexible field-effect transistors (FETs) with both unity—current gain frequencies, f_T, and unity—power gain frequencies, f_{max}, in the gigahertz frequency range.[3] Graphene is an ideal candidate for use in flexible radio frequency FETs (RF-FETs), as it offers both exceptional electronic and mechanical properties. Graphene demonstrates high room-temperature mobility (greater than 10 000 cm^2 V^{-1} s^{-1}) and carrier saturation velocity (1—5 × 10^7 cm s^{-1}),[4−6] as well as remarkable strain limits (25—35%).[7,8] Indeed, flexible graphene FETs (GFETs) have demonstrated f_T and f_{max} in the gigahertz frequency range.[9−13]

However, the cutoff frequencies realized in flexible GFETs have remained significantly below those of the best devices fabricated at equivalent channel lengths on rigid substrates.[14] Flexible GFETs have typically employed a bottom-gated device structure,[10,11] circumventing the need to integrate high-κ dielectric layers directly on the surface of graphene—a process that has remained challenging to date.[15,16] However, bottom-gated fabrication approaches present the lower surface of the graphene channel to dielectrics with high mechanical roughness and trapped charges while simultaneously leaving the top surface directly exposed to the surrounding environment. Substrate roughness,[17,18] trapped charges typically present in oxide-based dielectrics,[15,19] and atmospheric adsorbates[20] all contribute to increased scattering of charge carriers in the graphene channel, which degrades the electronic performance of GFETs. While encapsulation of flexible GFETs in organic or inorganic compounds has reduced environmental sensitivity, trapped charges introduced by the encapsulation process degrade the electronic properties of the underlying graphene and ultimately limit any benefit imparted to the GFET.[11,21−23] Indeed, poor electronic performance in conjunction with nonideal device structure has limited the achievable ratio of cutoff frequencies, f_{max}/f_T, to less than 0.6 in flexible

* Address correspondence to jh2228@columbia.edu.

Received for review May 9, 2015 and accepted August 11, 2015.

Published online August 11, 2015
10.1021/acsnano.5b02816

GFETs to date,[9−12] significantly below those achieved in GFETs fabricated on rigid substrates.[4] Simultaneously achieving both high f_T and f_{max}, represented by f_{max}/f_T approaching unity, is essential for practical analog and RF electronic applications,[3,24] with this ratio strongly influenced by dielectric materials in GFETs.[4,24,25] Integration of improved dielectric materials, both as gate dielectrics and surface passivation layers, which not only are flexible in form but also conserve the outstanding electronic properties of graphene, is essential to achieve improved performance in flexible GFETs.

Hexagonal boron nitride (hBN) is an ideal candidate as both a gate dielectric and encapsulation material for flexible GFETs. The dielectric properties of hBN (dielectric constant ∼3−4, dielectric breakdown strength ∼7.9 MV/cm^2) compare favorably with those of SiO_2.[26,27] Furthermore, hBN is a particularly suitable dielectric for use in graphene-based electronics; surface passivation of graphene by full encapsulation in hBN results in not only improved environmental stability of electronic properties[28,29] but also increased room-temperature mobility (in excess of 100 000 cm^2 V^{-1} s^{-1}).[30] In conjunction with a high mechanical strain limit,[31] the demonstrated enhancement to environmental stability and electronic performance of GFETs fabricated on rigid substrates suggests that hBN dielectrics hold the potential to transform the performance of flexible GFETs, as well.

RESULTS AND DISCUSSION

In this work, we fabricated GFETs with graphene channels fully encapsulated in hBN on flexible polyethylene naphthalate substrates. We achieve GFETs with channel lengths down to 375 nm by implementing a self-aligned fabrication scheme novel for flexible electronics. The electronic performance of flexible GFETs is characterized under both unstrained and strained conditions. Flexible GFETs fabricated with channel lengths of 2 μm demonstrate exceptional room-temperature carrier mobility (up to 10 000 cm^2 V^{-1} s^{-1}), strong current saturation characteristics (peak output resistance of 2000 Ω), and excellent mechanical flexibility (strain limits of 1%). Mobility and output resistance represent record values for flexible GFETs fabricated at any channel length. The high-frequency performance of flexible RF-FETs fabricated from hBN-encapsulated graphene at channel lengths of 375 nm is also presented. These devices demonstrate extrinsic cutoff frequencies f_T and f_{max} of 12.0 and 10.6 GHz, respectively, values only exceeded by flexible GFETs fabricated at shorter channel lengths.[9−13] The ratio of cutoff frequencies approaches unity (f_{max}/f_T = 0.9), an unprecedented value in flexible GFET technologies. Intrinsic f_T and f_{max} are revealed to be 29.7 and 15.7 GHz, respectively. This work demonstrates that hBN encapsulation of graphene not only improves DC and RF performance of flexible GFETs but also enables a novel, self-aligned fabrication scheme.

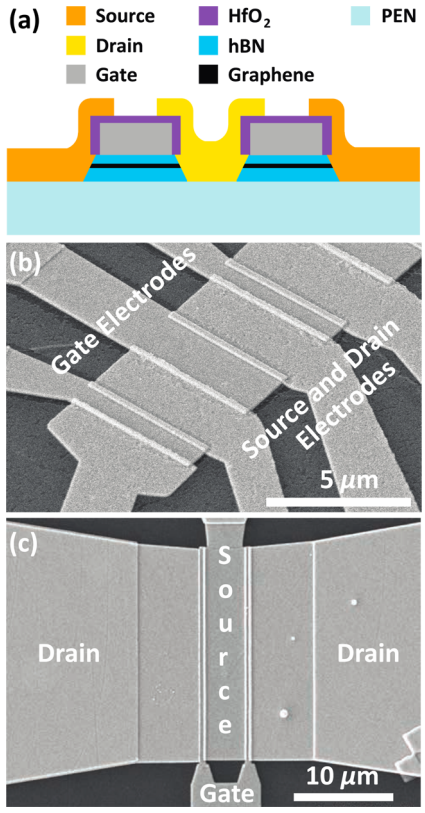

Figure 1. (a) Cross-sectional schematic of flexible GFETs fabricated using a self-aligned process. The graphene channel is fully encapsulated in hBN. (b,c) Scanning electron microscopy images of completed GFETs fabricated on flexible substrates. (b) Multiple, long-channel GFETs fabricated from a single hBN-encapsulated graphene (HGH) stack. GFETs have channel lengths of either 1 or 2 μm and channel widths of 5 μm. (c) Flexible, short-channel RF-FET fabricated with a dual-fingered gate structure. RF-FET has a channel length of 375 nm and an effective channel width of 20 μm.

Top-gated GFETs were fabricated on flexible substrates employing a novel, self-aligned fabrication scheme. Figure 1a shows a cross-sectional schematic of the self-aligned, flexible GFETs developed in this work (see Methods section for details on device fabrication).

GFETs characterized in this work were fabricated with two distinct device geometries. Long-channel GFETs were fabricated for purposes of DC characterization, with multiple two-terminal devices fabricated from a single hBN-encapsulated graphene (HGH) stack (bottom hBN thickness of 15.1 nm and top hBN thickness of 7.0 nm). Long-channel GFETs were fabricated with channel lengths of either 1 or 2 μm, channel widths of 5 μm, and source/drain gate overlap of ∼500 nm. For purposes of RF characterization, short-channel RF-FETs were fabricated with a dual-fingered gate and electrodes configured in a ground−signal−ground (GSG) coplanar waveguide structure. Flexible RF-FETs have a channel length of 375 nm, an effective channel width of 20 μm (two 10 μm gates in parallel), and source/drain

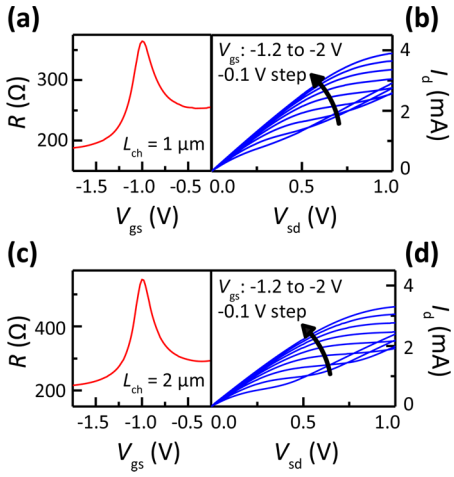

Figure 2. DC characteristics of flexible GFETs. (a,c) Device resistance, *R*, plotted as a function of gate-to-source voltage, V_{gs}. (c,d) Current−voltage (*I*−*V*) characteristics plotting drain current, I_d, as a function of source-to-drain voltage, V_{sd}. *I*−*V* curves are taken at fixed values of V_{gs} decreasing from −1.2 to −2 V in increments of −100 mV. Data are presented for a representative GFET fabricated with a channel length, L_{ch}, of 1 μm in (a,b), while data for a device with L_{ch} = 2 μm are plotted in (c,d). All devices are fabricated with channel widths of 5 μm.

gate overlap of ∼110 nm using the aforementioned self-aligned fabrication scheme. The flexible RF-FET was fabricated with a bottom hBN thickness of 23.7 nm and a top hBN thickness of 11.5 nm. The self-aligned fabrication scheme results in a device structure for which the gate length, channel length, and source−drain spacing are equivalent within detectable limits. Standard open and short de-embedding structures were simultaneously fabricated on-chip. Figure 1b,c shows scanning electron microscopy (SEM) images of completed long-channel GFETs (Figure 1b) and a short-channel RF-FET (Figure 1c) fabricated on flexible PEN substrates.

Electronic characteristics of long-channel GFETs were determined by two-terminal measurements conducted in ambient conditions. Figure 2a,c shows device resistance, *R*, plotted as a function of gate-to-source voltage, V_{gs}, measured at a fixed source-to-drain bias, V_{sd} = 10 mV, for representative flexible GFETs fabricated with channel lengths of 1 μm (Figure 2a) and 2 μm (Figure 2c). Side-contacted graphene devices previously fabricated on Si substrates with equivalent source and drain contacts (see Methods section for additional details) demonstrate lower electron contact resistance, in agreement with models predicting oxygen-terminated graphene edges.[30] Long-channel GFETs fabricated in this work demonstrate higher electron contact resistance, potentially indicative of process-related contamination at the electrode/graphene interface. Low-field, field-effect mobility was extracted from resistance data as $\mu_{FE} = (L_{ch}g_m)/(W_{ch}C_{tot}V_{sd})$, where L_{ch} is the channel length, W_{ch} is the channel width, g_m is the small-signal transconductance, and C_{tot} is the total effective gate capacitance per unit area. C_{tot} = 386 nF cm^{-2}, calculated as the series combination of the electrostatic capacitance ($C_e \approx 443$ nF cm^{-2}) and the quantum capacitance ($C_q \approx 3010$ nF cm^{-2}) over the pertinent carrier density range.[32] The dielectric constant, κ, for hBN is 3.5, as determined by prior work;[33] μ_{FE} = 4800 cm^2 V^{-1} s^{-1} for the GFET presented with a channel length of 1 μm. For the GFET with a channel length of 2 μm, μ_{FE} = 10 000 cm^2 V^{-1} s^{-1}, which represents the highest mobility demonstrated in a flexible GFET to date (regardless of channel length)[10−12,34−37] and comparable to values measured in the best GFETs fabricated on rigid substrates.[4]

Figure 2b,d presents high-bias current−voltage (*I*−*V*) characteristics for the same two flexible GFETs, for which the measured drain current, I_d, is plotted as a function of V_{sd} for fixed values of V_{gs} decreasing from −1.2 to −2 V. Peak g_m and r_0 extracted from the *I*−*V* characteristics of GFETs with channel lengths of both 1 and 2 μm are equivalent at 3.2 mS (0.64 mS/μm) and 2000 Ω, respectively (open-circuit voltage gain, $g_m \times r_0$ = 6.4). Peak g_m normalized by channel width exceeds the highest values achieved even in GFETs fabricated on rigid substrates with hBN dielectrics.[4] Flexible, hBN-encapsulated GFETs also demonstrated excellent *I*−*V* saturation characteristics, evident by the high value of r_0 achieved. The GFETs presented in this work demonstrate significantly improved mobility, transconductance, and output resistance in comparison with that of the best flexible GFETs previously reported using traditional oxide dielectrics (independent of channel length).[10−12,34−37] The improvements to electronic properties are attributed to the enhanced dielectric environment provided by hBN encapsulation.[15,30]

Next, mechanical limits of flexible GFETs fabricated with hBN dielectrics were determined. Electronic characteristics were measured while simultaneously applying uniaxial tensile strain, ε, along the axis perpendicular to the device channel under two-point bending. Figure 3 plots *I*−*V* characteristics at increasing levels of strain ranging from 0 to 1%. Strain-induced fluctuations in μ_{FE} result in less than 3% degradation (from the zero-strain value) at ε = 0.5% and less than 13% degradation at ε = 1%. Peak g_m exhibits less than 20% degradation from its unstrained value over the entire measured strain range (ε = 0−1%). Mechanical failure of flexible GFETs occurs at strains greater than ε = 1%, as observed by the measurement of open-circuit characteristics and indicative of mechanical failure occurring at the metal electrodes rather than the gate dielectric. Indeed, the source-to-gate current, I_{sg}, was measured to remain below 50 pA over the entire measured strain range, indicating negligible leakage current through the gate dielectric even under elevated levels of strain—in good agreement with both flexible MoS_2 FETs implementing hBN dielectrics[38] and experimental measurements of the strain limits of hBN films (greater than 3.0%).[31]

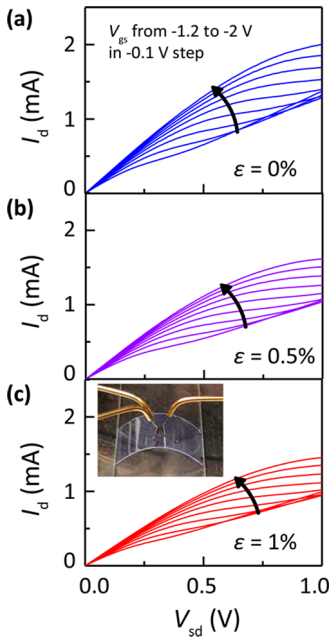

Figure 3. Current−voltage (I−V) characteristics plotting drain current, I_d, as a function of source-to-drain voltage, V_{sd}, taken at fixed values of gate-to-source voltage, V_{gs}, decreasing from −1.2 to −2 V in increments of −100 mV. Data are presented for increasing values of strain, ε, of (a) ε = 0%, (b) ε = 0.5%, and (c) ε = 1%. The inset of (c) shows an image of the measurement scheme in which a two-point bending setup is devised directly on the surface of a probe station. Data are presented for a flexible GFET with a channel length and width of 1 and 5 μm, respectively.

These results indicate that hBN functions as a robust gate dielectric for flexible GFETs with mechanical strain limits of at least 1%. Future dedicated studies are important to determine the upper strain limit of hBN dielectrics for use in flexible electronics.

In order to determine high-frequency performance of flexible, hBN-encapsulated GFETs, a short-channel RF-FET (shown in Figure 1c) was characterized under ambient conditions. DC characteristics of the flexible RF-FET were first measured, as presented in Figure 4. Figure 4a plots device resistance, R, as a function of V_{gs}, measured at a fixed drain-to-source bias, V_{ds} = 10 mV. The total effective gate capacitance per unit area, C_{tot}, for the device is 247 nF cm^{-2} ($C_e \approx$ 269 nF cm^{-2}, $C_q \approx$ 3010 nF cm^{-2}). Field-effect mobility is extracted from the resistance data as μ_{FE} = 2200 cm^2 V^{-1} s^{-1}. The device demonstrates lower electron contact resistance, characteristic for side-contacted GFETs with ideal electrode/graphene interfaces.[30] Figure 4b plots I−V characteristics of the flexible RF-FET. High-field values of g_m and r_0 are extracted from the I−V characteristics and plotted as a function of V_{gs} and V_{ds} in Figure 4c,d. Maximum g_m = 4.51 mS (0.23 mS/μm) and peak r_0 = 132.5 Ω are achieved at an equivalent bias point (V_{ds} = 0.5 V and V_{gs} = 1.5 V). The reduced values observed for μ_{FE}, g_m, and r_0 in comparison with that in long-channel GFETs presented earlier in this work follow channel length scaling trends observed in GFETs fabricated on rigid substrates.[15]

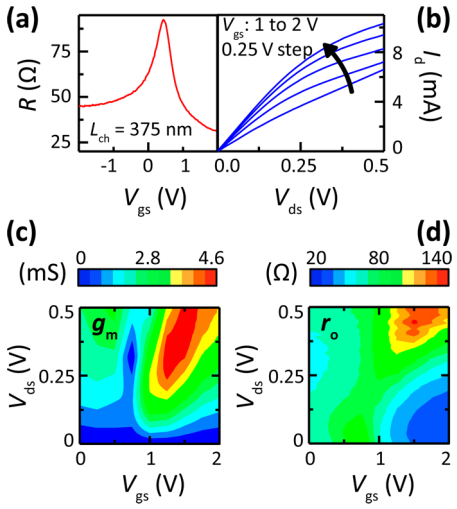

Figure 4. DC characteristics of a flexible, graphene RF-FET fabricated with a channel length of 375 nm and effective width of 20 μm. (a) Device resistance, R, plotted as a function of gate-to-source voltage, V_{gs}, measured at a fixed drain-to-source bias, V_{ds}, of 10 mV. (b) Current−voltage (I−V) characteristics plotting drain current, I_d, as a function of V_{ds}. I−V curves are taken at fixed values of V_{gs} increasing from 1 to 2 V in increments of 250 mV. (c) Transconductance, g_m, and (d) output resistance, r_0, plotted as a function of V_{ds} and V_{gs}.

Radio frequency characterization was subsequently conducted by measuring S-parameters from 100 MHz to 20 GHz on a two-port network analyzer. Figure 5a plots current gain (h_{21}) and unilateral power gain (U) as a function of frequency for the flexible RF-FET. Both h_{21} and U are measured at the bias point maximizing intrinsic gain (V_{ds} = 0.5 V, V_{gs} = 1.5 V; see Figure 4c,d). At this bias point, the device is operated as a unipolar n-type channel.

The device demonstrates extrinsic cutoff frequencies f_T and f_{max} of 12.0 and 10.6 GHz, respectively. These values represent the highest recorded extrinsic f_T and f_{max} for a flexible GFET fabricated at this channel length, with higher performance achieved only at channel lengths below 300 nm.[9−13,39] In comparison with the best flexible RF-FETs fabricated to date from MoS_2 (at channel lengths down to 68 nm),[40] the GFETs fabricated in this work demonstrate ∼2× improvement in extrinsic f_T and f_{max}. Furthermore, the ratio of extrinsic cutoff frequencies is close to unity (f_{max}/f_T = 0.9), significantly higher than previously achieved in any GFET fabricated on a flexible substrate (f_{max}/f_T < 0.6)[9−12] and equivalent to the best values achieved on Si substrates (f_{max}/f_T = 0.86).[4] The improved RF performance is attributed to the enhanced electronic performance afforded by full hBN encapsulation of the graphene channel and an optimized, self-aligned device structure.

Standard open and short de-embedding methods were implemented to enable direct comparison of the RF performance of the device presented in this work with previously reported GFETs analyzed using equivalent

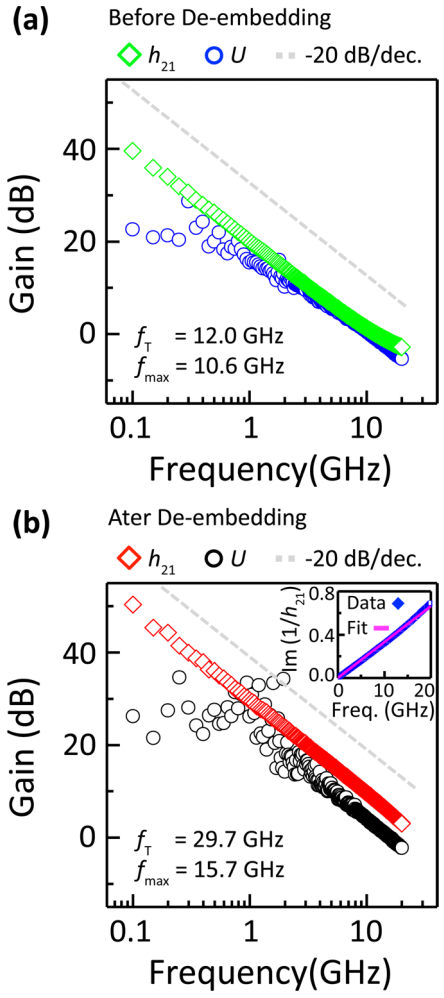

Figure 5. Radio frequency characteristics of a flexible graphene RF-FET. Current gain, h_{21}, and unilateral power gain, U, are plotted as a function of operation frequency both (a) prior to and (b) after de-embedding; extrinsic and intrinsic values of cutoff frequencies are presented, respectively. Dashed line indicates a −20 dB/dec slope, included to demonstrate that this frequency dependence is followed both prior to and after de-embedding. Inset of (b) plots Im($1/h_{21}$) as a function of frequency. The measured data (blue) are well fit by a linear regression (red). All RF data are presented for a device fabricated with a channel length of 375 nm and an effective channel width of 20 μm.

de-embedding procedures. Figure 5b plots h_{21} and U as a function of frequency after performing open and short de-embedding, revealing intrinsic f_T and f_{max} of 29.7 and 15.7 GHz, respectively. In order to verify the accuracy of the de-embedding methods implemented, f_T was indepenently calculated using Gummel's method.[14,41] The inset of Figure 5b plots Im($1/h_{21}$) as a function of frequency. The data are well fit by a linear regression from which f_T is extracted as 30.2 GHz, in excellent agreement with the value derived from a linear extrapolation of measured h_{21} (29.7 GHz; see Figure 5b). The difference between intrinsic and extrensic values of f_T are in line with GFETs characterized previoulsy in literature,[4,9,42] indicative of a similar magnitude of parasitic capacitances associated with the fabrication scheme implemented in this work. Further improvements to RF performance can be expected from additional channel length scaling and by minimization of the overlap between source/drain and gate electrodes, following similar trends for GFETs fabricated on rigid substrates.[14]

CONCLUSIONS

In conclusion, flexible GFETs are fabricated from graphene encapsulated in hBN using a self-aligned fabrication scheme novel for flexible electronics. Devices with channel lengths of 2 μm demonstrate exceptional carrier mobility (up to 10 000 $cm^2 V^{-1} s^{-1}$), high peak transconductance (0.64 mS/μm), and saturating $I-V$ characteristics (r_0 = 2000 Ω), representing record values for any flexible GFET to date. Flexible GFETs fabricated with channel lengths of 375 nm demonstrate μ_{FE} = 2200 $cm^2 V^{-1} s^{-1}$ and r_0 = 132.5 Ω. Extrinsic cutoff frequencies are f_T = 12.0 GHz and f_{max} = 10.6 GHz, with the ratio of cutoff frequencies approaching unity (f_{max}/f_T = 0.9). RF performance is unprecedented for a flexible GFET fabricated at this channel length and only exceeded in devices fabricated at shorter channel lengths.[12,39] The outstanding DC and RF performance is attributed to the enhanced dielectric environment provided by full hBN encapsulation of the graphene channel in conjunction with an optimized, self-aligned device structure. Furthermore, hBN-encapsulated GFETs demonstrate high mechanical flexibility with strain limits of at least 1%. These results demonstrate that hBN is a mechanically robust dielectric that can afford enhanced electronic characteristics to a wide array of graphene-based, flexible electronics.

METHODS

GFETs were fabricated on 127 μm thick polyethylene naphthalate (PEN) substrates. To facilitate device processing, PEN substrates were first adhered onto Si handle substrates using a film of polydimethylsiloxane as an adhesive layer (6 μm thickness), implementing a process described in prior literature.[39] The hBN-encapsulated graphene (HGH) stacks were prepared from exfoliated graphene and hBN crystals followed by subsequent transfer onto PEN substrates using procedures described previously in detail.[30] HGH stacks utilized in this work were assembled with a bottom hBN thicknesses of ∼20 nm, top hBN thicknesses of ∼10 nm, and graphene of monolayer thickness.

Following HGH stack preparation, GFETs were fabricated with top-gate electrodes (1 nm Ti/20 nm Pd/80 nm Au) defined by electron beam lithography and lift-off. The gate contact pad was subsequently thickened with a second metal evaporation (1 nm Ti/50 nm Au). Next, a conformal HfO_2 dielectric (10 nm thickness) was grown over the gate electrode by atomic layer deposition (ALD) at 150 °C. The higher surface activation energy

of hBN in comparison with that of the metal gate electrode resulted in a selective ALD deposition;[43−46] a continuous layer of HfO_2 was deposited only on the metal gate electrode but not on the hBN dielectric surface. These findings are corollary to previous work demonstrating that chemical functionalization is prerequisite for successful ALD deposition of dielectrics on graphene, a molecule which presents an equivalent covalently bonded and chemically inert surface.[16,47]

The HGH stack was etched ∼10 nm below the graphene layer in an inductively coupled plasma (ICP) of CHF_3 and O_2 gases. The top-gate was used as an etch mask, resulting in a channel geometry both defined by and self-aligned to the gate electrode. Because HfO_2 is not etched by the ICP process, the selective ALD-deposited passivation layer remained covering the gate electrode. Source and drain electrodes (1.5 nm Cr/20 nm Pd/80 nm Au) were evaporated to form side contacts with the graphene channel.[30] Self-alignment of the source and drain electrodes was achieved by allowing their overlap with the gate electrode; selective HfO_2 passivation of the gate prevents electrical contact between the overlapping source/drain and gate electrodes and is thus critical to enabling this self-aligned fabrication scheme. The contact pad regions of the source and drain electrodes were thickened by an additional metal evaporation (1 nm Ti/50 nm Au) to complete device fabrication.

All dimensions of GFETs and de-embedding structures were verified by SEM to ensure fidelity of the fabrication process. The hBN layer thicknesses were determined by atomic force microscopy (AFM) measurements. Exfoliated graphene samples were verified to be a monolayer thick by Raman spectroscopy. After transfer onto PEN substrates, HGH stacks were confirmed to be free of structural defects by AFM prior to device fabrication. Upon completion of GFET fabrication, flexible PEN substrates were mechanically released from Si handles prior to electronic characterization.

Conflict of Interest: The authors declare no competing financial interest.

Acknowledgment. This work was funded by the Air Force Office of Scientific Research (AFOSR) Multidisciplinary University Research Initiative (MURI) Program on new graphene materials technology under Grant FA9550-09-1-0705 and by the Defense Advanced Research Projects Agency (DARPA) under U.S. Office of Naval Research Contract N00014-1210814.

REFERENCES AND NOTES

1. Mannoor, M. S.; Tao, H.; Clayton, J. D.; Sengupta, A.; Kaplan, D. L.; Naik, R. R.; Verma, N.; Omenetto, F. G.; McAlpine, M. C. Graphene-Based Wireless Bacteria Detection on Tooth Enamel. *Nat. Commun.* **2012**, *3*, 763.
2. Kim, D. H.; Lu, N.; Ma, R.; Kim, Y. S.; Kim, R. H.; Wang, S.; Wu, J.; Won, S. M.; Tao, H.; Islam, A.; et al. Epidermal Electronics. *Science* **2011**, *333*, 838–843.
3. Akinwande, D.; Petrone, N.; Hone, J. Two-Dimensional Flexible Nanoelectronics. *Nat. Commun.* **2014**, *5*, 5678.
4. Meric, I.; Dean, C. R.; Petrone, N.; Wang, L.; Hone, J.; Kim, P.; Shepard, K. L. Graphene Field-Effect Transistors Based on Boron-Nitride Dielectrics. *Proc. IEEE* **2013**, *101*, 1609–1619.
5. Shishir, R. S.; Ferry, D. K. Velocity Saturation in Intrinsic Graphene. *J. Phys.: Condens. Matter* **2009**, *21*, 344201.
6. Perebeinos, V.; Avouris, P. Inelastic Scattering and Current Saturation in Graphene. *Phys. Rev. B: Condens. Matter Mater. Phys.* **2010**, *81*, 195442.
7. Lee, C.; Wei, X.; Kysar, J. W.; Hone, J. Measurement of the Elastic Properties and Intrinsic Strength of Monolayer Graphene. *Science* **2008**, *321*, 385–388.
8. Wei, X.; Fragneaud, B.; Marianetti, C. A.; Kysar, J. W. Nonlinear Elastic Behavior of Graphene: *Ab Initio* Calculations to Continuum Description. *Phys. Rev. B: Condens. Matter Mater. Phys.* **2009**, *80*, 205407.
9. Sire, C.; Ardiaca, F.; Lepilliet, S.; Seo, J. W.; Hersam, M. C.; Dambrine, G.; Happy, H.; Derycke, V. Flexible Gigahertz Transistors Derived from Solution-Based Single-Layer Graphene. *Nano Lett.* **2012**, *12*, 1184–1188.
10. Petrone, N.; Meric, I.; Hone, J.; Shepard, K. L. Graphene Field-Effect Transistors with Gigahertz-Frequency Power Gain on Flexible Substrates. *Nano Lett.* **2013**, *13*, 121–125.
11. Lee, J.; Ha, T. J.; Li, H. F.; Parrish, K. N.; Holt, M.; Dodabalapur, A.; Ruoff, R. S.; Akinwande, D. 25 GHz Embedded-Gate Graphene Transistors with High-K Dielectrics on Extremely Flexible Plastic Sheets. *ACS Nano* **2013**, *7*, 7744–7750.
12. Yeh, C. H.; Lain, Y. W.; Chiu, Y. C.; Liao, C. H.; Moyano, D. R.; Hsu, S. S. H.; Chiu, P. W. Gigahertz Flexible Graphene Transistors for Microwave Integrated Circuits. *ACS Nano* **2014**, *8*, 7663–7670.
13. Zhu, W.; Farmer, D. B.; Jenkins, K. A.; Ek, B.; Oida, S.; Li, X. S.; Bucchignano, J.; Dawes, S.; Duch, E. A.; Avouris, P. Graphene Radio Frequency Devices on Flexible Substrate. *Appl. Phys. Lett.* **2013**, *102*, 233102.
14. Wu, Y.; Jenkins, K.; Valdes-Garcia, A.; Farmer, D. B.; Zhu, Y.; Bol, A.; Dimitrakopoulos, C.; Zhu, W.; Xia, F.; Avouris, P.; et al. State-of-the-Art Graphene High-Frequency Electronics. *Nano Lett.* **2012**, *12*, 3062–3067.
15. Meric, I.; Dean, C. R.; Young, A. F.; Baklitskaya, N.; Tremblay, N. J.; Nuckolls, C.; Kim, P.; Shepard, K. L. Channel Length Scaling in Graphene Field-Effect Transistors Studied with Pulsed Current-Voltage Measurements. *Nano Lett.* **2011**, *11*, 1093–1097.
16. Wang, X.; Tabakman, S. M.; Dai, H. Atomic Layer Deposition of Metal Oxides on Pristine and Functionalized Graphene. *J. Am. Chem. Soc.* **2008**, *130*, 8152–8153.
17. Lui, C. H.; Liu, L.; Mak, K. F.; Flynn, G. W.; Heinz, T. F. Ultraflat Graphene. *Nature* **2009**, *462*, 339–341.
18. Katsnelson, M. I.; Geim, A. K. Electron Scattering on Microscopic Corrugations in Graphene. *Philos. Trans. R. Soc., A* **2008**, *366*, 195–204.
19. Wang, H.; Wu, Y.; Cong, C.; Shang, J.; Yu, T. Hysteresis of Electronic Transport in Graphene Transistors. *ACS Nano* **2010**, *4*, 7221–7228.
20. Schedin, F.; Geim, A. K.; Morozov, S. V.; Hill, E. W.; Blake, P.; Katsnelson, M. I.; Novoselov, K. S. Detection of Individual Gas Molecules Adsorbed on Graphene. *Nat. Mater.* **2007**, *6*, 652–655.
21. Some, S.; Kim, J.; Lee, K.; Kulkarni, A.; Yoon, Y.; Lee, S.; Kim, T.; Lee, H. Highly Air-Stable Phosphorus-Doped n-Type Graphene Field-Effect Transistors. *Adv. Mater.* **2012**, *24*, 5481–5486.
22. Shin, W. C.; Seo, S.; Cho, B. J. Highly Air-Stable Electrical Performance of Graphene Field Effect Transistors by Interface Engineering with Amorphous Fluoropolymer. *Appl. Phys. Lett.* **2011**, *98*, 153505.
23. Alexandrou, K.; Petrone, N.; Hone, J.; Kymissis, I. Encapsulated Graphene Field-Effect Transistors for Air Stable Operation. *Appl. Phys. Lett.* **2015**, *106*, 113104.
24. Schwierz, F. Graphene Transistors: Status, Prospects, and Problems. *Proc. IEEE* **2013**, *101*, 1567–1584.
25. Wu, Y.; Farmer, D. B.; Xia, F.; Avouris, P. Graphene Electronics: Materials, Devices, and Circuits. *Proc. IEEE* **2013**, *101*, 1620–1637.
26. Dean, C. R.; Young, A. F.; Meric, I.; Lee, C.; Wang, L.; Sorgenfrei, S.; Watanabe, K.; Taniguchi, T.; Kim, P.; Shepard, K. L.; et al. Boron Nitride Substrates for High-Quality Graphene Electronics. *Nat. Nanotechnol.* **2010**, *5*, 722–726.
27. Lee, G. H.; Yu, Y. J.; Lee, C.; Dean, C.; Shepard, K. L.; Kim, P.; Hone, J. Electron Tunneling through Atomically Flat and Ultrathin Hexagonal Boron Nitride. *Appl. Phys. Lett.* **2011**, *99*, 243114.
28. Wang, L.; Chen, Z.; Dean, C. R.; Taniguchi, T.; Watanabe, K.; Brus, L. E.; Hone, J. Negligible Environmental Sensitivity of Graphene in a Hexagonal Boron Nitride/Graphene/h-BN Sandwich Structure. *ACS Nano* **2012**, *6*, 9314–9319.
29. Mayorov, A. S.; Gorbachev, R. V.; Morozov, S. V.; Britnell, L.; Jalil, R.; Ponomarenko, L. A.; Blake, P.; Novoselov, K. S.; Watanabe, K.; Taniguchi, T.; et al. Micrometer-Scale Ballistic Transport in Encapsulated Graphene at Room Temperature. *Nano Lett.* **2011**, *11*, 2396–2399.
30. Wang, L.; Meric, I.; Huang, P. Y.; Gao, Q.; Gao, Y.; Tran, H.; Taniguchi, T.; Watanabe, K.; Campos, L. M.; Muller, D. A.; et al.

One-Dimensional Electrical Contact to a Two-Dimensional Material. *Science* **2013**, *342*, 614–617.
31. Song, L.; Ci, L.; Lu, H.; Sorokin, P. B.; Jin, C.; Ni, J.; Kvashnin, A. G.; Kvashnin, D. G.; Lou, J.; Yakobson, B. I.; et al. Large Scale Growth and Characterization of Atomic Hexagonal Boron Nitride Layers. *Nano Lett.* **2010**, *10*, 3209–3215.
32. Meric, I.; Han, M. Y.; Young, A. F.; Ozyilmaz, B.; Kim, P.; Shepard, K. L. Current Saturation in Zero-Bandgap, Top-Gated Graphene Field-Effect Transistors. *Nat. Nanotechnol.* **2008**, *3*, 654–659.
33. Young, A. F.; Dean, C. R.; Meric, I.; Sorgenfrei, S.; Ren, H.; Watanabe, K.; Taniguchi, T.; Hone, J.; Shepard, K. L.; Kim, P. Electronic Compressibility of Layer-Polarized Bilayer Graphene. *Phys. Rev. B: Condens. Matter Mater. Phys.* **2012**, *85*, 235458.
34. Lee, S. K.; Jang, H. Y.; Jang, S.; Choi, E.; Hong, B. H.; Lee, J.; Park, S.; Ahn, J. H. All Graphene-Based Thin Film Transistors on Flexible Plastic Substrates. *Nano Lett.* **2012**, *12*, 3472–3476.
35. Lu, C. C.; Lin, Y. C.; Yeh, C. H.; Huang, J. C.; Chiu, P. W. High Mobility Flexible Graphene Field-Effect Transistors with Self-Healing Gate Dielectrics. *ACS Nano* **2012**, *6*, 4469–4474.
36. Kim, B. J.; Jang, H.; Lee, S. K.; Hong, B. H.; Ahn, J. H.; Cho, J. H. High-Performance Flexible Graphene Field Effect Transistors with Ion Gel Gate Dielectrics. *Nano Lett.* **2010**, *10*, 3464–3466.
37. Lee, J.; Tao, L.; Hao, Y.; Ruoff, R. S.; Akinwande, D. Embedded-Gate Graphene Transistors for High-Mobility Detachable Flexible Nanoelectronics. *Appl. Phys. Lett.* **2012**, *100*, 152104.
38. Lee, G. H.; Yu, Y. J.; Cui, X.; Petrone, N.; Lee, C. H.; Choi, M. S.; Lee, D. Y.; Lee, C.; Yoo, W. J.; Watanabe, K.; et al. Flexible and Transparent MoS2 Field-Effect Transistors on Hexagonal Boron Nitride-Graphene Heterostructures. *ACS Nano* **2013**, *7*, 7931–7936.
39. Petrone, N.; Meric, I.; Chari, T.; Shepard, K. L.; Hone, J. Graphene Field-Effect Transistors for Radio-Frequency Flexible Electronics. *IEEE J. Electron Devices Soc.* **2015**, *3*, 44–48.
40. Cheng, R.; Jiang, S.; Chen, Y.; Liu, Y.; Weiss, N.; Cheng, H. C.; Wu, H.; Huang, Y.; Duan, X. Few-Layer Molybdenum Disulfide Transistors and Circuits for High-Speed Flexible Electronics. *Nat. Commun.* **2014**, *5*, 5143.
41. Gummel, H. K. On the Definition of the Cutoff Frequency fT. *Proc. IEEE* **1969**, *57*, 2159.
42. Wang, H.; Hsu, A. L.; Palacios, T. Graphene Electronics for RF Applications. *IEEE Microw. Mag.* **2012**, *13*, 114–125.
43. Hammer, B.; Norskov, J. K. Why Gold Is the Noblest of All the Metals. *Nature* **1995**, *376*, 238–240.
44. Canning, N. D. S.; Outka, D.; Madix, R. J. The Adsorption of Oxygen on Gold. *Surf. Sci.* **1984**, *141*, 240–254.
45. Zhang, Z.; Guo, W. Controlling the Functionalizations of Hexagonal Boron Nitride Structures by Carrier Doping. *J. Phys. Chem. Lett.* **2011**, *2*, 2168–2173.
46. Zhao, Y.; Wu, X.; Yang, J.; Zeng, X. C. Oxidation of a Two-Dimensional Hexagonal Boron Nitride Monolayer: A First-Principles Study. *Phys. Chem. Chem. Phys.* **2012**, *14*, 5545–5550.
47. Meric, I.; Dean, C. R.; Han, S. J.; Wang, L.; Jenkins, K. A.; Hone, J.; Shepard, K. L. High-Frequency Performance of Graphene Field Effect Transistors with Saturating IV-Characteristics. *Technol. Dig. Int. Electron Devices Meeting* **2011**, 2.1.1–2.1.4.